SLAC-PUB-3317
April 1984
(I)

A NEW DRIFT CHAMBER FOR THE MARK II AT SLC*

GAIL G. HANSON
Stanford Linear Accelerator Center
Stanford University, Stanford, California 94305

Summary

A new cylindrical drift chamber is being constructed for the Mark II detector for use at the new SLAC Linear Collider. The design of the new chamber is based on a multi-sense-wire cell of the jet-chamber type. In addition to drift-time measurements, pulse height measurements from the sense wires will provide electron-hadron separation by dE/dx. The design and construction of the chamber, tests of prototypes, and chamber electronics are discussed.

Introduction

The Mark II detector,[1] which has run successfully at both the SPEAR and PEP e^+e^- storage rings at SLAC, is being upgraded to be the first detector at the new SLAC Linear Collider (SLC).[2] The design of the first detector for the SLC is severely constrained by the time schedule. The SLC is scheduled to turn on for physics in January, 1987. The first detector must be rugged, reliable, and checked out at PEP – both hardware and software – and must be ready to produce physics at the SLC by January, 1987. Since the move from PEP to the SLC takes about a year, the detector must be ready to run at PEP by January, 1985, in order to take data during the Spring and Fall running cycles.

The new drift chamber forms the heart of the Mark II detector for the SLC,[3] shown in Fig. 1. We will describe here briefly the components of the detector. The drift chamber is cylindrical and is supported inside a 5 kG conventional solenoidal magnet. The magnet flux return iron is unchanged from the present detector, which limits the outer radius of the drift chamber. The magnet coil will be replaced with a new one of similar design. Between the coil and the drift chamber are new scintillation counters used in the trigger and to measure time of flight. The lead and liquid argon electromagnetic calorimeter surrounding the coil will be unchanged from the present detector. New endcap gas electromagnetic calorimeters are being built. The muon identification system is unchanged. At the SLC there will be a new vertex detector and small-angle luminosity monitor.

Drift Chamber Design

Our primary goal in designing the new drift chamber was compatibility with the physics we expect to do at the Z^0. The general considerations were:

1. Good momentum resolution in a 5 kG magnetic field,
2. Good solid angle coverage,
3. Ease of pattern recognition and high tracking efficiency at the Z^0, and
4. dE/dx as an independent aid to calorimetry for electron-hadron separation for momenta less than about 10 GeV/c.

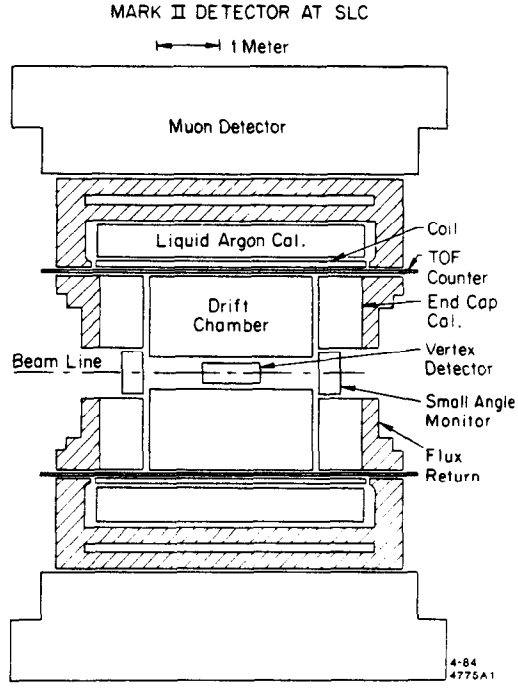

Fig. 1. Plan view of the Mark II detector for SLC.

Cell Design

The design of the drift chamber is based on a multi-sense-wire cell, shown in Fig. 2, which is a shortened version of the jet-chamber configuration.[4] The half-width of the cell, 3.3 cm in the center, was constrained by the effect of diffusion on position resolution for a gas at atmospheric pressure. The length was chosen to be large enough to give good electric field uniformity. The uniformity achieved can be seen in Fig. 3, which shows the drift trajectories of electrons produced along a particle path. The drift trajectories are very straight, resulting in a linear time-distance relationship. Only one side of each endmost wire shows appreciable deviation from linearity, and corrections of 2 ns (100 μm) will be needed here. This good linearity helps provide good accuracy in pattern recognition and track fitting.

The cell contains six sense wires staggered ± 380 μm from the cell axis to provide local left-right ambiguity resolution. The spacing between sense wires is 8.33 mm. We made this distance as small as we thought was practical in order to get a small double track separation, which is approximately half the sense wire spacing. There are two guard wires on either end of the cell for shaping the electric field and equalizing the gains

* Work supported by the Department of Energy, contract DE-AC03-76SF00515.

Invited talk presented at the 3rd International Conference on Instrumentation for Colliding Beam Physics, Novosibirsk, U.S.S.R., March 15-21, 1984

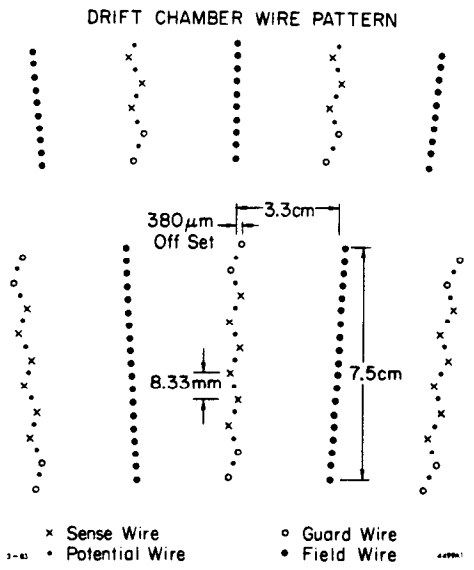

Fig. 2. Drift chamber cell structure.

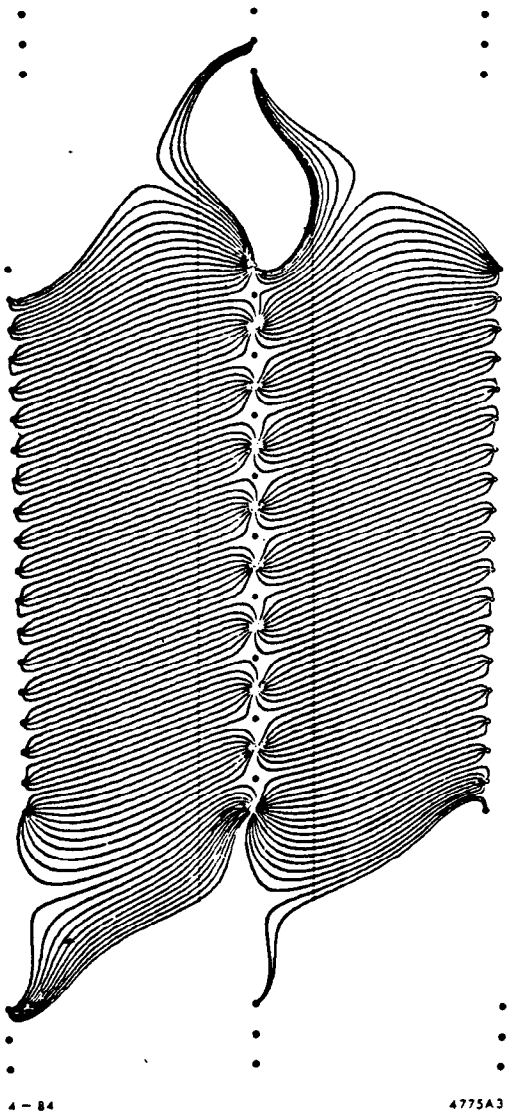

Fig. 3. Electron drift trajectories in drift chamber cell.

of the sense wires. Potential wires are placed between the sense wires to control the gain of the sense wires, reduce the signal coupling between adjacent sense wires, and reduce the electrostatic deflection of the sense wires. With zero charge on the potential wires the electrostatic deflection of the staggered sense wires is 72 μm in the center of the chamber. This deflection can be almost completely canceled by putting sufficient voltage on the potential wires. This provides a configuration with very stable wire positions but also results in a reduced drift electric field which may not be optimal for achieving saturated drift velocity and small Lorentz angle. We plan to operate the chamber with reduced but not canceled electrostatic deflection, depending on the gas chosen. The signal coupling between adjacent sense wires is about 7%. (It would be 17% without the potential wires.) The sense wires are 30 μm diameter gold-plated tungsten and are tensioned to 113 gm to give 91 μm gravitational sag in the center of the 2.45 m overall length. The potential and guard wires are 102 μm gold-plated Inconel 600, tensioned to have the same gravitational sag as the sense wires.

There are nineteen field-wires in each cell with 4.16 mm spacing. They are made of 178 μm gold-plated beryllium-copper. The end wire has a larger diameter (305 μm) in order to keep the field below about 20 kV/cm on the surface of the wire to prevent whisker growth.

Chamber Design

The drift chamber consists of twelve concentric cylindrical layers of cells. Alternate layers have their wires parallel to the cylinder axis or at $\approx \pm 3.8°$ to the cylinder axis to provide stereo information. (The stereo angle is achieved by stringing the wires with an offset of five half-cells between the two ends.) The angular offsets between the starting points of the cell patterns in the axial layers were adjusted to maximize the distance between tracks and the sense and field wire positions. The radial distance between layers is maintained at 2.5 cm minimum, including the displacement of stereo wires toward the center in the middle of the stereo layers, in order to control the change in gain as cells in adjacent stereo and axial layers change their relative orientation. The active length of the chamber is 2.30 m. The overall chamber layout is shown in Fig. 4 and the design parameters are given in Table I. There are a total of 5832 sense wires and 72 measurements of drift time and dE/dx for tracks traversing the full radial extent of the chamber.

Mechanical Design

The wires will be strung between 2-inch aluminum endplates. The wires pass through slots in the endplates for each row of nineteen wires in a cell. The endplates are held apart by a 2 mm thick beryllium inner cylinder and by a 1/2-inch thick cylindrical aluminum outer shell. The inner radius of the drift chamber is 19.2 cm and the outer radius is 151.9 cm. The ends of the inner cylinder are aluminum epoxied to the beryllium. The outer shell has four large windows for access. The windows are closed with 1/4-inch panels. The inner and outer cylinders are welded to the endplates. The endplates will be prestrained to keep the wire tension uniform. The inner and outer cylinders are lined with copper-clad kapton to which high

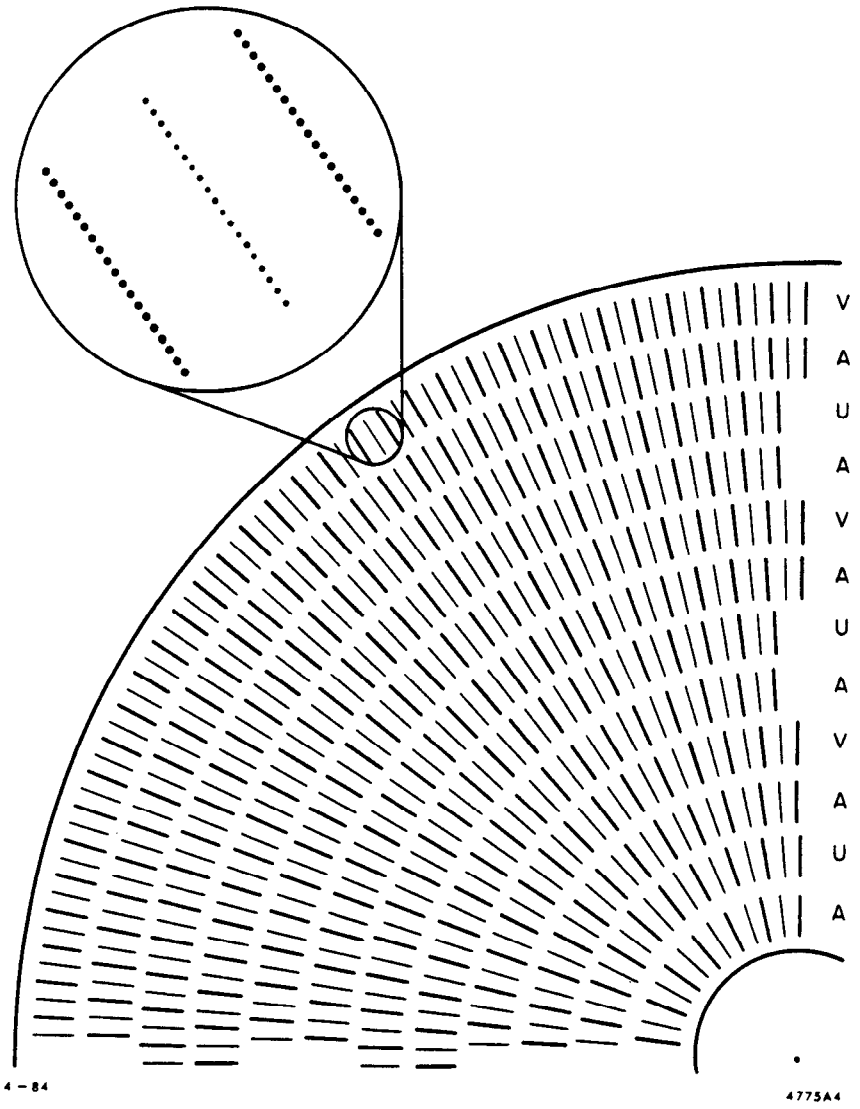

Fig. 4. Overall layout of the drift chamber.

TABLE I. Drift Chamber Parameters

Layer	Radius at Center (*cm*)	Stereo Angle (*degrees*) Wire 1	Wire 6	Number of Cells
1	27.05	0	0	26
2	38.25	3.65	4.07	36
3	48.45	0	0	46
4	59.25	-3.73	-4.00	56
5	69.45	0	0	66
6	80.15	3.76	3.96	76
7	90.35	0	0	86
8	100.95	-3.77	-3.93	96
9	111.15	0	0	106
10	121.65	3.77	3.91	116
11	131.85	0	0	126
12	142.35	-3.78	-3.89	136

voltage is applied to maintain a uniform electric field in the inner and outer drift chamber layers.

All the wires in one row of a cell are positioned by a one-piece injection-molded Delrin 500*AF* feedthrough, shown in Fig. 5. The feedthroughs are epoxied into the slots in the endplates. The inside of the slot in the aluminum is insulated with an injection-molded polysulfone sleeve. Each feedthrough is located on the endplate by pinning to three accurately-machined holes in both the feedthrough and the endplate. The wires are located in machined notches along one side of a central slot in the feedthrough, tensioned, and soldered to a printed circuit board epoxied to the Delrin feedthrough. For added assurance, the ends of the wires are epoxied to a strip of kapton which is epoxied over the printed circuit board. We expect to locate wires to $\pm$ 35 μm. Sources of errors in wire location are the following: feedthrough accuracy in machining and placement - 15 μm, error in endplate machining and placement - 25 μm, and error in wire sag and electrostatic deflection - 10 μm. The open slot in the feedthrough permits the wires to be strung in

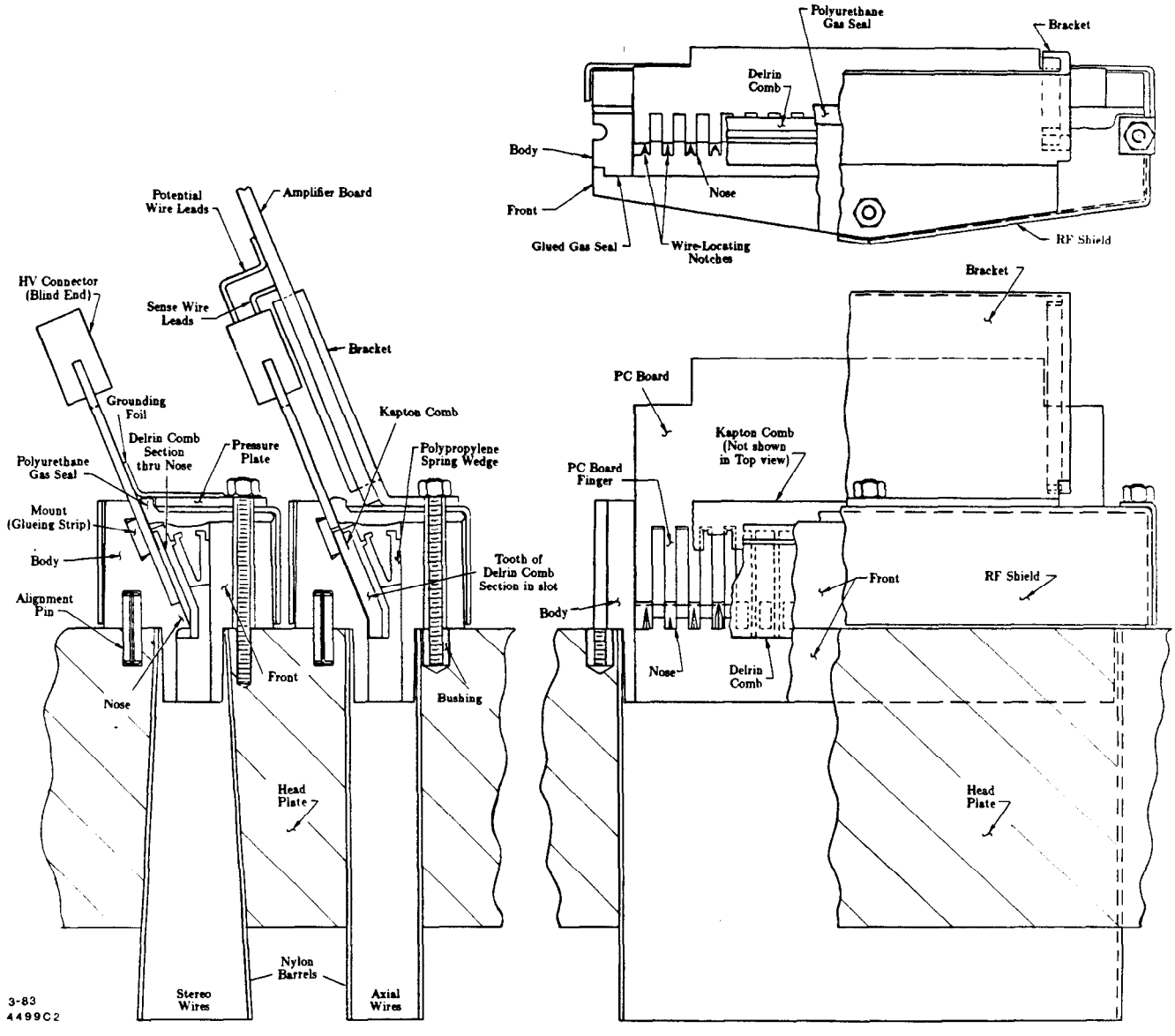

Fig. 5. Feedthrough design.

groups, which saves time in wire stringing. The slot also allows access for replacement of single wires, if necessary, and provides for visual inspection of the interior. Replacement of wires after the chamber is built can be accomplished by attaching them to a sacrifical field wire or potential wire which can be used to pull the wire, plus a replacement for the sacrifical wire, through the chamber. The gas seal over the slot is accomplished with a silicone gasket and a brass pressure plate. Electrical connections to the wires are made through the printed circuit board.

At the time of this talk (March, 1984), the endplates had been drilled and a sample of feedthrough alignment holes had been measured. The measured holes agreed with the specifications to about 25 μm *rms*. The endplates were in the process of alignment and welding to the outer shell. The feedthrough parts had been manufactured and the machined notches and alignment holes were found to be within tolerances for the samples measured. Feedthroughs were being assembled. Stringing was expected to start in about a month.

High Voltage

The drift electric field is determined primarily by the voltages on the field wires. The voltage on the potential wires determines the gain of the sense wires. The voltage on the guard wires helps to control the uniformity of gain of the six sense wires.

A graded high voltage is supplied to each cell through a resistor-divider chain. The voltage must be graded to provide a uniform drift field over the varying width of the cell. The width variation is different in each layer. The nineteen field wires in each cell are ganged to form nine sets of wires, each of which is at the same voltage, without introducing significant distortions in the drift field. One high-voltage power supply supplies field-wire voltage to an entire layer. The voltage on a field wire in the center of a cell is typically - 4.8 kV, depending on the gas used. The potential wire and guard wire voltages are typically - 1.5 kV and - 200 V, respectively.

Tracking and Momentum Resolution

We expect to measure positions from drift times to an accuracy of 200 μm or better. The position resolution is determined principally by details of the electron drift in the gas. We expect a contribution from diffusion of the order of 150 μm, depending on the drift distance. As was mentioned previously, we expect the error from wire placement to be 35 μm. The position error due to the electronics should be about 1 ns (50 μm for typical drift velocities).

We will record multiple hits on each wire. By paying careful attention to pulse shaping, we should obtain a double track resolution of 3-4 mm.

The local resolution of left-right ambiguities and the nearly linear space-time relation facilitate tracking at the pattern recognition stage. Furthermore, comparison of the times from several wires in a cell allows the use of the very good resolution of the chamber for the rejection of spurious hits (multiple-pulsing, single bremsstrahlung hits, poorly measured points due to δ-rays, confused points due to crossing tracks in the cell) before pattern recognition begins. This could be particularly useful in an environment containing many soft photons or neutrons which might give a fair number of single hits but very few compatible hits over a number of adjacent wires. Finally, the randomization of the wire pattern from layer to layer improves our ability to separate nearby tracks and guarantees that a track cannot everywhere be very near sense or field wires where the measurement accuracy tends to be worst.

Based on the expected position resolution of 200 μm, we predict a momentum resolution of $\sigma(p)/p^2 \leq 0.15\%\ GeV^{-1}$ over 70% of the solid angle using a constraint that the tracks originate at the beam interaction point. This increases to $0.45\%\ GeV^{-1}$ at $\cos\theta = 0.85$, where θ is the polar angle. Multiple scattering is expected to contribute an additional error of $\sigma(p)/p = 1.4\%$. There are at least twenty measurements per track over 90% of the solid angle. The resolutions in azimuthal and polar angle are $\approx 0.1\ mr$ and $\approx 1.2\ mr$, respectively, over 70% of the solid angle using a vertex constraint. Tracking algorithms are presently being studied using Monte Carlo simulations.

dE/dx Measurement

dE/dx information is obtained from pulse height measurement of the sense wire signals. The drift chamber will provide 72 samples of 8.33 mm size. We have estimated the resolution to be 6.9% for the gas 89% argon/10% CO_2/1% methane, using the calculations of Va'Vra.[5] The dE/dx separation between particles of different types is given by the quantity $\Delta E/\sigma$, where ΔE is the difference in dE/dx between the particles and σ is the resolution. The separation for electrons and pions, muons, kaons, and protons as a function of particle momentum is shown in Fig. 6 (a). Since there are regions of ambiguity, time-of-flight information in conjunction with dE/dx provides considerable improvement. We find that the separation is better than three standard deviations for momenta up to 6 GeV/c. For 80% electron tagging efficiency a 10 to 1 pion rejection can be expected for momenta up to 12.5 GeV/c. Even if we achieve only a 10% dE/dx resolution, the same pion rejection can be obtained up to 7.5 GeV/c. Kaon identification using dE/dx and time of flight is shown in Fig. 6 (b). There is identification power at the 1.5 standard deviation level up to 10 GeV/c.

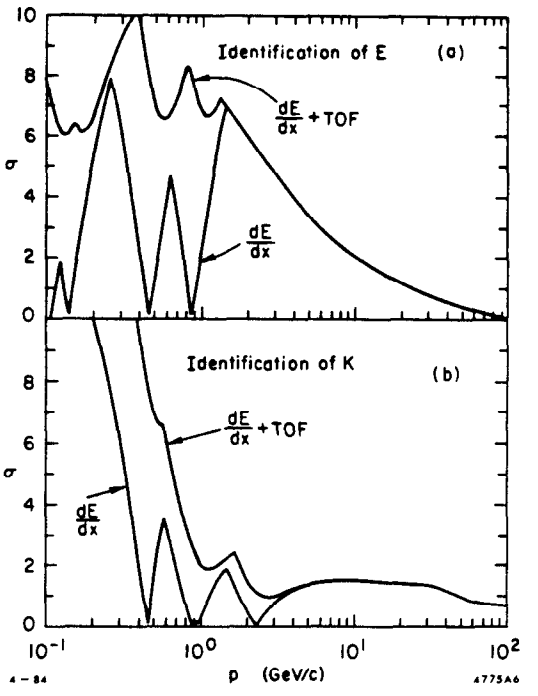

Fig. 6. dE/dx identification as a function of momentum for (a) electrons and (b) kaons.

The 10:1 electron-pion separation from dE/dx and time of flight is in addition to the electron identification already provided by the electromagnetic calorimetry. The dE/dx identification is particularly useful for particles in the center of jets. Using the lead-liquid-argon calorimeters alone the hadron rejection rate is expected to be 20:1 in the center of a jet at the Z^0 compared with 200:1 for isolated electrons. Using the dE/dx information in addition increases the rejection rate to > 500:1 even in the core of a jet. The improved electron identification capability will allow us to obtain larger samples of events from semileptonic decays of heavy quarks with smaller background contamination, especially for b quarks. As has already been shown with the Mark II at PEP, electron tagging is a powerful tool for obtaining samples of events for lifetime measurements using a vertex chamber. In addition, dE/dx information can be used to reduce the minimum separable distance between double tracks by a factor of two.

Pulse height corrections are needed to attain the 6.9% dE/dx resolution. Some of the most serious corrections are mentioned here:

1. At a gain of 5×10^4 saturation corrections of 25% for tracks at 90° to the sense wires are expected, with smaller corrections at other angles. We plan to run at a gain $\leq 5 \times 10^4$.
2. Cross talk between adjacent sense wires is 7% but will be reduced to the 1% level with decoupling resistors.
3. Gain variation along the length of the sense wire due to the crossing of axial and stereo layers is expected to be

±7% for the edge wires and < 1% for the inner wires in a cell.

4. Distortions in the drift trajectories and differences in collection region can produce a gain change of ±10% for the edge sense wires.

5. Temperature and pressure variations change the density of the gas and therefore the ion statistics. Experience with Mark III at SPEAR has shown that a 1% change in absolute temperature or pressure produces a 6% change in gain. Temperature and pressure will be monitored to make these corrections.

6. Impurities in the gas, particularly oxygen, can degrade the gain. Control of leaks in the chamber and monitoring of the gas gain with a small chamber should allow us to keep these corrections small.

7. Variation in the diameter of the sense wire produces a 3% change in gain for a 1% change in sense wire diameter. We are using wire with a 0.5% tolerance in diameter.

Drift Chamber Prototyping

Gas and Position Resolution Studies

We have built a full-length one-cell prototype (actually several) which we have used to study electrostatic stability, comparison of gains with electrostatics simulations, noise reduction, electronics, decoupling resistors, pole-zero filters, and position resolution. A separate small chamber was used to study electron drift velocities in various gases as a function of drift field. In addition, we have carried out prototyping studies of wire positioning, high-voltage standoff, and gas sealing for the feedthroughs.

We have considered gases composed of mixtures of argon, CO_2, and methane, motivated by the success of the High Resolution Spectrometer at PEP and the Mark III at SPEAR with the mixture 89% argon/10% CO_2/1% methane. We have also made measurements with 50% argon/50% ethane, which is in wide use but has given problems with whisker growth and high current draw. We have considered only those gases whose drift velocity remains constant with changes in drift field for drift fields near 1000 V/cm. Figure 7 shows drift velocities as a function of drift field for the gases considered. One of our goals has been to find a suitable gas with relatively low drift velocity ($\approx$ 30 $\mu m/ns$) in order to minimize the contribution to position resolution from time-resolution effects such as rise time, time slewing, time walk, and a fixed time-resolution bin and to minimize the contribution of the $1/t$ tail of the drift chamber pulse to the double track separation. In addition, the Lorentz angle is proportional to the drift velocity. Another advantageous property of some of the gases is the increase in drift velocity as the drift field decreases. The provides a focusing effect since the electrons with the longest drift trajectories are those which pass near the potential wires where the electric field is lower and speeding them up produces a narrower pulse and thus better double track separation.

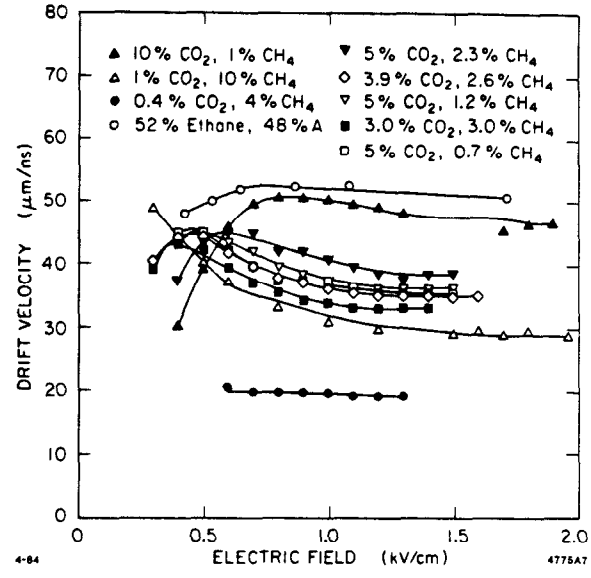

Fig. 7. Drift velocity versus electric field for various gases.

Of course, we are most concerned with obtaining the best possible position resolution. As mentioned previously, the largest contribution to position resolution is diffusion, which affects the position resolution both close to the wire and proportional to $\sqrt{x}$, where x is the drift distance. Position resolutions were measured with cosmic ray data in the one-cell prototype. The position resolution for an individual wire was measured by fitting to the width of the double-peaked distribution found when plotting the quantity $(t_1+t_3)/2-t_2$, where t_1, t_2, and t_3 are the drift times measured for a staggered triplet of wires. An example of such a distribution is shown in Fig. 8. The double peak is due to tracks passing on either side of the sense wire plane. The distance between the peaks is twice the stagger between the sense wires divided by the drift velocity. For each gas the position resolution was measured as a function of distance between the track and the wire, as shown in Fig. 9. The data were fitted to the form

$$\sigma^2 = \sigma_0^2 + D^2 x.$$

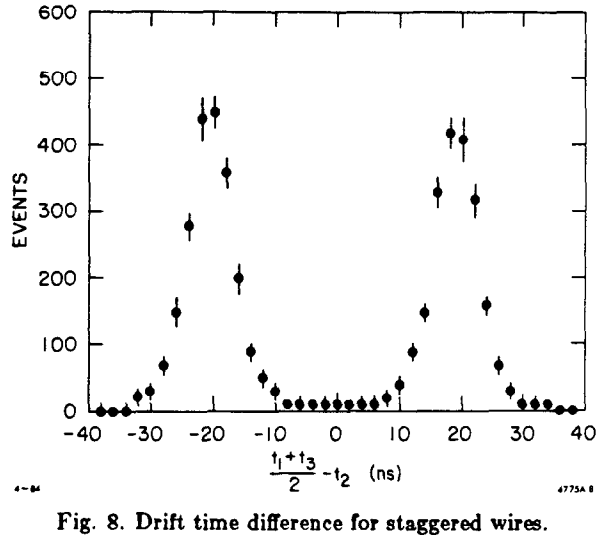

Fig. 8. Drift time difference for staggered wires.

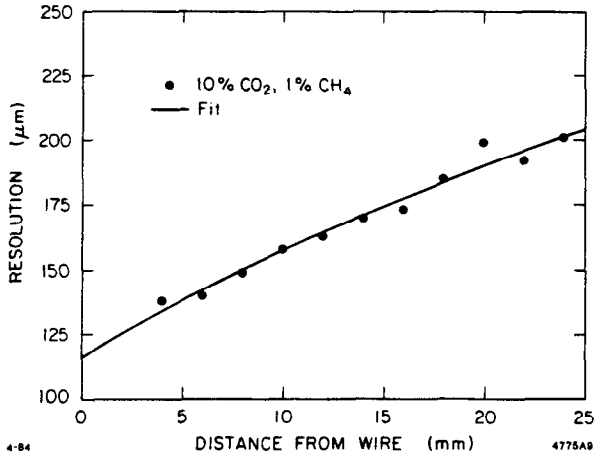

Fig. 9. Position resolution versus drift distance for 89% argon/ 10% CO_2/1% methane.

In addition, the average position resolution across the cell $<\sigma>$ was calculated. The parameters found for the different gases are listed in Table II. The measurements were made for a constant average pulse height from the drift chamber (2.7 mV at the preamp input). The general trend is that the average position resolution increases as the percentage of argon increases, presumably because argon has the largest diffusion coefficient. 50% argon/50% ethane has the best position resolution.

Unfortunately, another factor which must be considered is gas stability. A small chamber was built to study whisker growth and large current draw under conditions of large fields on the surface of field wires. (Whiskers are polymerized hydrocarbons which grow from field wires to sense wires.) While these conditions are extreme, they may give some indication of how well a chamber will operate with these gases. All gases with more that 5% methane grew whiskers. 50% argon/50% ethane drew excess current at high voltage which continued when the voltage was lowered.

The conclusions from these tests were that position resolutions less than 200 μm could be obtained with this cell design and that, of the gases tested, 89% argon/10% CO_2/1% methane and 92.5% argon/5% CO_2/2.5% methane are the best candidates for use in the chamber in terms of position resolution, double track separation, and gas stability. Further gas studies are being carried out.

dE/dx Studies

Integrated pulse heights were measured for the sense wires in the one-cell prototype for cosmic rays using a LeCroy 2249W ADC. Saturation as a function of gain on the sense wire was measured. The ratio of pulse heights, corrected for path length, at 90° to the sense wires and at 65° to the sense wires is plotted versus charge on the sense wires in Fig. 10. 108% of nominal charge corresponds to the gain used in the resolution studies

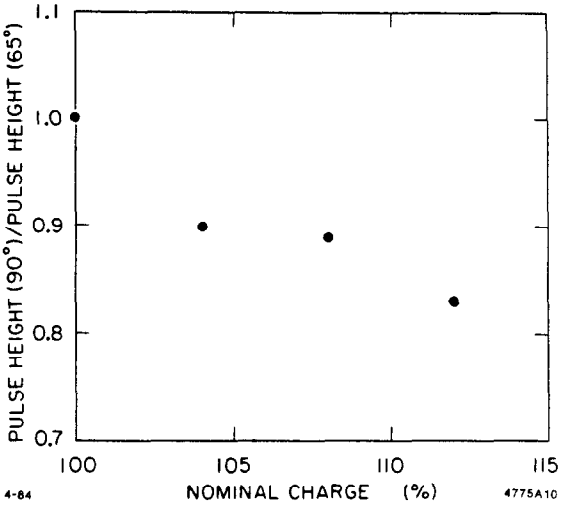

Fig. 10. Corrected ratio of pulse heights at 90° to sense wires and at 65° to sense wires versus charge on the sense wires.

TABLE II. Drift Chamber Prototype Gas Studies

Gas Composition			E_d	v_d	σ_0	D	$<\sigma>$
% CO_2	% Methane	% Argon	(V/cm)	($\mu m/ns$)	(μm) (±5)	($\mu m/\sqrt{cm}$) (±4)	(μm) (±6)
10.0	1.0	89.0	900	51.0	116	106	176
1.0	10.0	89.0	1000	32.2	108	115	179
5.0	2.5	92.5	1000	41.0	130	111	190
3.9	2.6	93.5	1000	36.3	127	127	203
5.0	1.2	93.8	1000	37.5	125	122	197
3.0	3.0	94.0	1000	32.0	115	139	207
5.0	0.7	94.3	1000	37.0	149	123	215
0.4	4.0	95.6	800	19.2	118	152	222
50% Ethane, 50% Argon			900	52.0	92	73	130

reported in the previous section. The gas used was 89% argon/ 10% CO_2/1% methane. A saturation effect of 11% was seen at the gain at which we would probably operate. This would correspond to a saturation effect of 20% over the full range of angles over which we would operate. The saturation measured agrees with that seen by Va'Vra[6] at a gain of 4×10^4.

A 50-*cm*-long chamber consisting of three layers of three cells each, shown in Fig. 11, has been built to study dE/dx measurement. The top and bottom layers are stereo layers and the middle layer is axial. Data taking with the chamber has just begun in an electron test beam.

Chamber Electronics

A block diagram of the drift chamber electronics is shown in Fig. 12. The preamplifiers are mounted and shielded directly on the drift chamber endplate. The postamplifiers are located in boxes mounted near the drift chamber on the magnet iron. The drift times and pulse heights are measured by FASTBUS modules in the electronics house. Data is read out through Scanner/Processor modules and a FASTBUS Interface by the existing VAX-11/780 computer. More information on the data acquisition can be obtained from Reference 7.

Preamplifiers

The preamplifier design is based on the Plessey SL560C chip. There are six channels per board, corresponding to the six sense wires in a drift chamber cell. The preamplifiers have undergone extensive development and testing on the one-cell prototype. Some of the specifications are as follows:

1. The voltage gain is 23.
2. The input noise is 25 μV *rms*, as measured on the drift chamber.
3. The risetime is 8 *ns*.

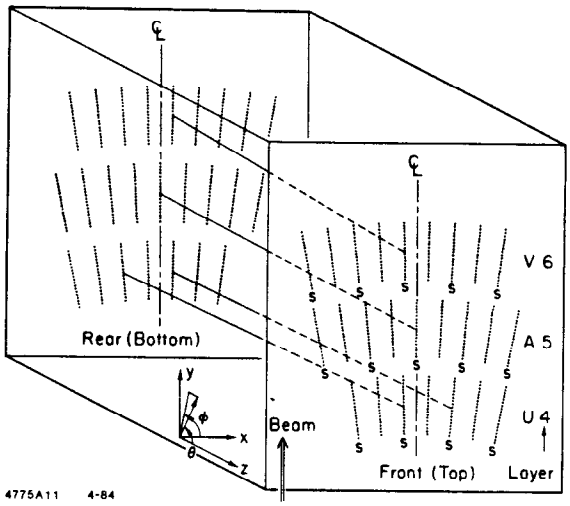

Fig. 11. dE/dx test chamber.

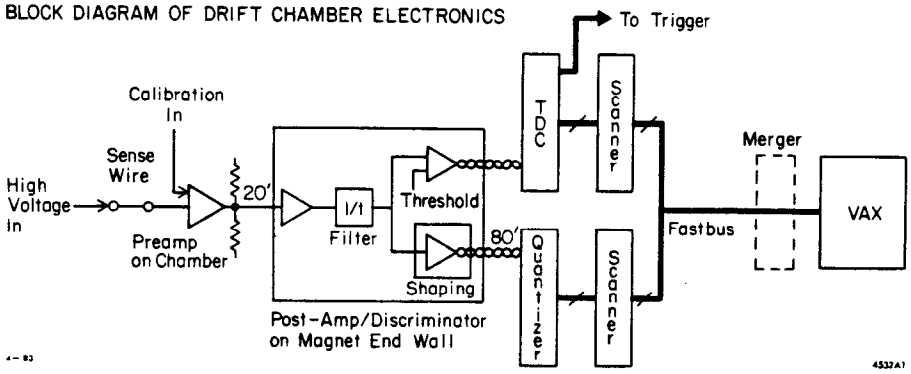

Fig. 12. Block diagram of drift chamber electronics.

4. The preamplifier contains crosstalk canceling resistors to reduce the crosstalk between adjacent sense wires and next-to-adjacent sense wires to the level of less than 1.5%. They feed an attenuated negative signal from a sense wire to cancel the positive signal from the drift chamber crosstalk.
5. The linearity is $\pm$ 6% for input signals of 0.5 to 20 mV.
6. The baseline shift is less than 1.5 % using a drift chamber pulse.
7. The overshoot is less than 10%
8. Power dissipation is 100 mW per channel.
9. Fanout of a calibration signal to each channel is accomplished.

The preamplifiers are now in production.

Postamplifier/Discriminator

The postamplifier further amplifies the drift chamber pulse, shapes the pulse to cancel the $1/t$ tail from the drift chamber pulse and the distortions introduced by the long cables to the electronics house, splits the pulse for timing and dE/dx measurement, and discriminates the pulse for the timing channel. Some of the specifications are listed here:

1. A two-stage pole-zero filter cancels the $1/t$ tail.
2. The gain is 1000 for the timing channel and variable in steps from 28 to 418 for the dE/dx channel. Gain uniformity is $\pm$10% in both channels.
3. The risetime is less than 10 ns.
4. The nonlinearity is less than $\pm$10% in the timing channel and less than $\pm$3% in the dE/dx channel.
5. The discriminator is a LeCroy MVL407 comparator with output pulse width given by time over threshold.
6. The calibration pulse is fanned out to the preamplifiers.
7. There is separate cable compensation for the timing and dE/dx channels. The timing channel error from cable distortion is less than 1 ns in the second pulse of a pair when the interval between the trailing edge of the first pulse and the leading edge of the second pulse is 20 ns or greater. The dE/dx error should be less than 2% after 100 ns measured from the leading edge of a 40-ns-wide square pulse.

The postamplifier design is almost complete. A prototype version is being used in the beam test setup.

Time Digitization

The drift times will be digitized by LeCroy 1879 TDC's. These TDC's are newly developed FASTBUS modules based on a silicon-on-sapphire shift register. There are 96 channels per module. The nominal bin width is 2 ns, although the clock speed can be modified. A final version from LeCroy has been tested. The measured time resolution was less than 1 ns, with channel-to-channel correlation less than 0.4 ns.[2] Twenty modules are due to be delivered in April. Complete electronics for time measurement is scheduled to be ready by Fall 1984.

dE/dx Electronics

The design of the dE/dx electronics is not yet final. We are planning to digitize the pulse height using 6-bit 100 MHz Flash ADC's. The Siemens SDA 5200 and TRW TDC1029 are being considered. Another possibility is the LeCroy MV200 Analog Shift Register which runs at 50 MHz (but could be used at 100 MHz with two channels clocked on opposite clock phases). The output from the shift register could be digitized with an 8-bit slow ADC. The design goal is 24 channels per FASTBUS module because of rack space limitations, but there are still problems with power and/or space limitations on the board. The dE/dx electronics is expensive: the budget estimate is \$1.16 M with 18 channels/module.

The schedule goals are to instrument approximately one-sixth of the chamber for running at PEP in 1985 and to have the full system operational at SLC by January, 1987.

Scanner/Processor

The Scanner/Processor, being developed at SLAC, controls the readout of the FASTBUS modules - the TDC's and dE/dx modules. It performs the Segment Interconnect functions. It is programmable in IBM assembly language. The Scanner/Processor module accomplishes sparse scan, pedestal and gain corrections, and other preprocessing of the data. A prototype is being built.

Conclusion

We expect to have the drift chamber and timing electronics ready for a cosmic-ray test in mid-November, 1984. The detector will be moved into the interaction region at PEP in January, 1985, for checkout. Using data taken at PEP we expect to get the tracking programs operational and gain some experience with dE/dx measurement before the move to SLC beginning in January, 1986. If the chamber performs as designed, we will be able to carry out a very exciting physics program at the SLC.

References

1. R. H. Schindler, *et al.*, Phys. Rev. D 24, 78 (1981).
2. SLAC Linear Collider Conceptual Design Report, SLAC-229, June, 1980.
3. Proposal for the Mark II at SLC, CALT-68-1015, April, 1983.

   The collaboration for the Mark II at the SLC consists of physicists from U. C. Santa Cruz, Caltech, University of Colorado, University of Hawaii, Johns Hopkins University, Lawrence Berkeley Laboratory, University of Michigan, and SLAC Groups A, C, E, and BC.
4. W. Farr, *et al.*, Nucl. Instr. and Meth. 156, 283 (1978).
5. J. Va'Vra, SLC Note CN-12.
6. J. Va'Vra, L. Roberts, D. Freytag, and P. Clancey, SLAC-PUB-2882.
7. A. J. Lankford and T. Glanzman, Proceedings of the Nuclear Science Symposium, San Francisco, CA, October, 1983, SLAC-PUB-3241.